Soft Matter

PAPER

Cite this: *Soft Matter*, 2018, **14**, 1939

Highly-organized stacked multilayers *via* layer-by-layer assembly of lipid-like surfactants and polyelectrolytes. Stratified supramolecular structures for (bio)electrochemical nanoarchitectonics†

M. Lorena Cortez, *[a] Agustín Lorenzo,[a] Waldemar A. Marmisollé,[a] Catalina von Bilderling,[a] Eliana Maza,[a] Lía Pietrasanta,[bc] Fernando Battaglini,[d] Marcelo Ceolín[a] and Omar Azzaroni *[a]

Received 6th January 2018,
Accepted 18th February 2018

DOI: 10.1039/c8sm00052b

rsc.li/soft-matter-journal

Supramolecular self-assembly is of paramount importance for the development of novel functional materials with molecular-level feature control. In particular, the interest in creating well-defined stratified multilayers through simple methods using readily available building blocks is motivated by a multitude of research activities in the field of "nanoarchitectonics" as well as evolving technological applications. Herein, we report on the facile preparation and application of highly organized stacked multilayers *via* layer-by-layer assembly of lipid-like surfactants and polyelectrolytes. Polyelectrolyte multilayers with high degree of stratification of the internal structure were constructed through consecutive assembly of polyallylamine and dodecyl phosphate, a lipid-like surfactant that act as a structure-directing agent. We show that multilayers form well-defined lamellar hydrophilic/hydrophobic domains oriented parallel to the substrate. More important, X-ray reflectivity characterization conclusively revealed the presence of Bragg peaks up to fourth order, evidencing the highly stratified structure of the multilayer. Additionally, hydrophobic lamellar domains were used as hosts for ferrocene in order to create an electrochemically active film displaying spatially-addressed redox units. Stacked multilayers were then assembled integrating redox-tagged polyallylamine and glucose oxidase into the stratified hydrophilic domains. Bioelectrocatalysis and "redox wiring" in the presence of glucose was demonstrated to occur inside the stratified multilayer.

Introduction

Interfacial supramolecular assemblies generated in layer-by-layer (LbL) fashion have sparked great interest owing to their potential applications in a wide range of research fields.[1–5] An important cornerstone for the construction of multicomponent interfacial architectures is the development of methods for integrating molecular building blocks into well-defined organized assemblies.[6–9] Research efforts on this matter are often referred to as "nanoarchitectonics", a term popularized by Ariga and co-workers.[10–17] It is now widely accepted that the LbL of polyelectrolytes represents a valuable technique for the fabrication of thin functional films of composition controlled at the nanometer scale. However, the interpenetration of successively adsorbed polyelectrolyte layers that is responsible for altering the local structure of the multilayer can be described as a scrambled egg polyelectrolyte complex rather than a truly layered, stratified film.[18] More specifically, no Bragg reflections appear in X-ray reflectograms of such "multilayered" films, except when some special polyelectrolytes capable of forming lyotropic mesophases are being used.[19] In these exceptional cases, these special polyelectrolytes are responsible for the formation of an ordered film structure extending over long distances. On the other hand, Bragg peaks may also appear in X-ray reflectograms when

[a] *Instituto de Investigaciones Fisicoquímicas Teóricas y Aplicadas (INIFTA), Departamento de Química, Facultad de Ciencias Exactas, Universidad Nacional de La Plata – CONICET, La Plata, Argentina. E-mail: lcortez@inifta.unlp.ed.ar, azzaroni@inifta.unlp.edu.ar; Web: https://softmatter.quimica.unlp.edu.ar*

[b] *Instituto de Física de Buenos Aires (IFIBA, UBA-CONICET), Facultad de Ciencias Exactas y Naturales, Universidad de Buenos Aires, C1428EHA Buenos Aires, Argentina*

[c] *Centro de Microscopías Avanzadas, Facultad de Ciencias Exactas y Naturales, Universidad de Buenos Aires, C1428EHA Buenos Aires, Argentina*

[d] *Instituto de Química Física de los Materiales, Medio Ambiente y Energía (INQUIMAE), Universidad de Buenos Aires – CONICET, Argentina*

† Electronic supplementary information (ESI) available. See DOI: 10.1039/c8sm00052b

the organic polyanion is replaced by negatively charged inorganic platelets such as clay or titanate platelets.[20–25] Up to date, only few heterosupramolecular systems have demonstrated perfect assemblies indicated by the presence of high-order Bragg reflections: CdS in polyelectrolytes,[26] CdTe in phospholipids,[27] rigid cellulose crystals and flexible polyallylamine,[28] and gold nanoparticles integrated in spin-assisted LbL assemblies.[29] Regarding this latter example, it is necessary to consider that despite valuable research efforts to obtain stratified polyelectrolyte multilayers with organized internal structure *via* spray or SA-LbL deposition,[26,30–32] the main strategy to control the stratification of polyelectrolyte multilayers still relies on limiting the interdiffusion of layers by introducing inorganic[33,34] or cross-linked "buffer" layers.[35–37] Very recently, Zapotoczny and co-workers demonstrated the creation of polyelectrolyte multilayers with stratification of the internal structure through assembly of statistical amphiphilic copolyelectrolytes of opposite charges.[38] In this regard, the integration of amphiphilic/micellar building blocks in LbL assemblies has been explored by several groups and facilitated the incorporation of small water-insoluble molecules into the interfacial architecture.[39–43] These research activities, in turn, led to a general, versatile, and robust route to bringing hydrophobic domains into thin films processed in aqueous solutions. However, the stratification of polyelectrolyte multilayers displaying well-organized hydrophobic domains derived from the assembly of micellar architectures remains elusive.

In a similar vein, multilayer assemblies containing redox-active enzymes are also of great interest within the scientific community as they are versatile architectures to create bioelectrochemical sensors or even biomimetic signal-transfer systems.[44–46] A further challenge in the growing area of "nanoarchitectonics" is the creation of new methodologies for the spontaneous assembly of molecular building blocks onto solid surfaces in predetermined arrangements for the fabrication of functional 3D-assemblies.[47–49] This aspect is particularly relevant if we consider that well-organized, multilayered, stacked nanoarchitectures – like lipid membranes – are a common principle in many biological systems to spatially organize processes and compartmentalize molecules.

Recently, Jeuken and his collaborators[50] reported the construction of multilayers of membrane enzymes in a native-like lipid environment using the LbL assembly of bacterial membrane extracts on gold electrodes. The potential of lipid-containing polyelectrolyte multilayers to mimic complex multilayer membrane assemblies is remarkable,[51–53] yet the development of consistent methodologies to attain such well-organized nanoassemblies has been limited. Only few model systems has been described to consistently show the existence of well-defined, stratified lipid domains. On the other hand, despite the versatility of lipids to offer different amphiphilicity as well as diversity of head and tail chemistry, they are relatively expensive and delicate building blocks and demand the formation of stable vesicles or extruded liposomes prior to their integration in the polyelectrolyte assembly. With this background in mind, our motivation was to develop a simple, robust and reproducible strategy to build up stratified PEMs displaying functional features, including biological activity, in spatially addressed domains, without requiring the use of inorganic structuring agents, but retaining the ease and generality of the traditional LbL assembly. A main aim was to demonstrate that (bio)functional hosts can be deliberately located in stratified domains without disrupting the intrinsic nanoorganization of the supramolecular assemblies, thus leading to the formation of "functional (bio)supramolecular stratified assemblies" *via* soft-chemical nanoarchitectonics.[54]

Herein, we report for the first time the fabrication of stratified functional PEMs using lipid-like surfactants as structure-directing agents. The formation of complex interfacial architectures displaying localized functional nanospaces with distinct hydrophobic/hydrophilic properties allowed selective incorporation of ferrocene (Fc) into the aliphatic domains. On the other hand, although multilayer integration of electroactive polyelectrolytes and redox enzymes have been described, to the best of our knowledge reports on truly layered, stratified bioelectroactive films have been missing yet. For such systems, we demonstrate bioelectrocatalytic properties arising from the "wiring" of the enzymes hosted in the stratified hydrophilic domains across the films. The obtained data indicate that the integration of lipid-like surfactants in polyelectrolyte multilayers provides not only a simple and reproducible strategy for producing stratified heterosupramolecular assemblies, but also offers a complementary perspective from which one can consider the manipulation of the supramolecular organization of multicompartmentalized interfacial architectures.

Results and discussion

Multilayer films were fabricated by alternating deposition of poly(allylamine) hydrochloride (PAH) and sodium dodecylphosphate (DP). The regular deposition of DP/PAH bilayers on a silicon substrate was confirmed based on thickness measurements using ellipsometry. Fig. 1 displays the thickness of DP/PAH films *versus* the number of deposited layers obtained from ellipsometry experiments. The layer-by-layer formation of the film shows a linear dependence on the number of layers and the deposition process is reproducible from layer to layer.

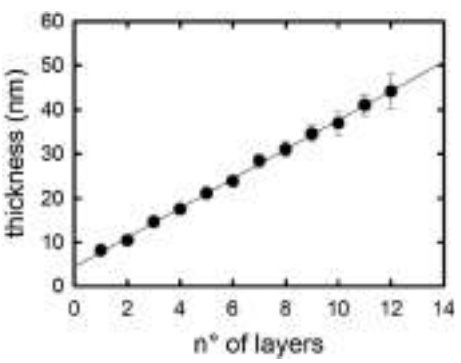

Fig. 1 Ellipsometric thickness of the dodecyl phosphate/polyallylamine multilayers on silicon surfaces *vs.* the number of deposited layers. Odd and even layer numbers correspond to dodecyl phosphate and polyallylamine layers, respectively.

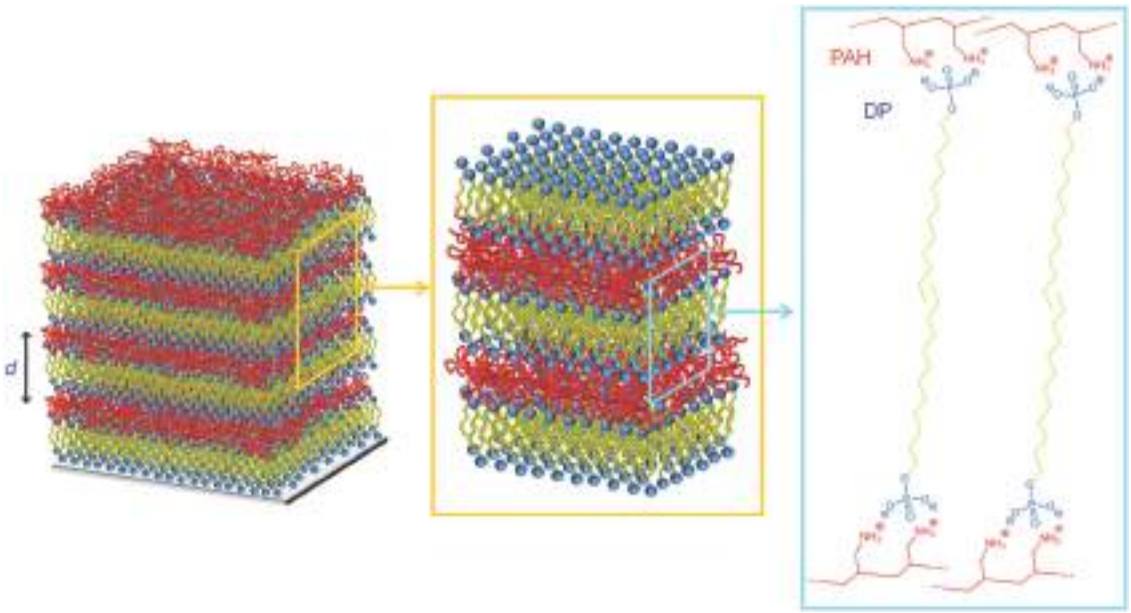

Scheme 1 Schematic representation of the supramolecular nanoorganized structures generated *via* layer-by-layer assembly of stratified dodecyl phosphate/polyallylamine.

The ellipsometric measurement indicated that the thickness of each DP/PAH bilayer was 6.6 ± 0.4 nm, in full agreement with XRR results (see below). When considering the successive thickness increments, each DP layer contributes with 4.0 ± 0.5 nm whereas the increment due to the PAH component is 2.6 ± 0.3 nm. According to these values, the thickness of each DP layer formed during each assembly step agrees well with the formation of a lipid-like bilayer exhibiting a tail-to-tail arrangement (see Scheme 1).

The mesostructural features and internal organization of the LbL films were then characterized by X-ray reflectivity (XRR). This nondestructive technique provides nanoscopic information about the thickness of the layers constituting the thin film, and it offers advantages over ellipsometry in that accurate information about the dimensional characteristics of buried layers can be obtained. Fig. 2 shows the X-ray reflectivity data corresponding to the DP/PAH multilayers. The presence of sharp Bragg diffraction peaks up to the fourth order proves a well-stratified layering and indicates highly oriented lamellar structures as deduced from the reciprocal spacing ratio (q/q^*), 1 : 2 : 3 : 4. Considering the chemical nature of the assembled building blocks, the lamellar nanostructure of the polyelectrolyte/surfactant multilayer can be described as a microphase-separated molecular system consisting of an ionic phase and a non-ionic phase. The ionic phase contains the poly-electrolyte chains and the ionic phosphate groups of the surfactants, whereas the non-ionic phase contains the hydrophobic alkyl chains (Scheme 1).

The narrow form of the peaks together with the high number of Bragg reflections indicate that films formed are internally well-organized at the molecular and mesoscopic level. The efficient ''structure-directing'' character of dodecyl-phosphate molecules is likely accountable for the remarkable

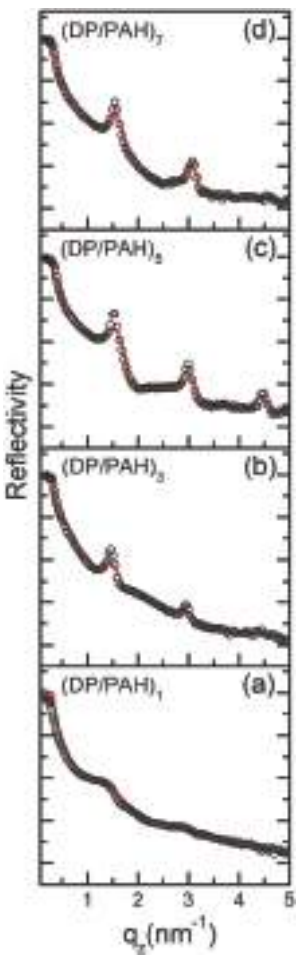

Fig. 2 Specular X-ray reflectivity curves (empty circles) together with a fit to the data (solid red line) from: (a) $(DP/PAH)_1$, (b) $(DP/PAH)_3$, (c) $(DP/PAH)_5$, (d) $(DP/PAH)_7$ multilayers. The X-ray structural data corroborates the formation of a stratified interfacial architecture with nanoscale periodicity.

internal organization, leading to the compartmentalization of polyelectrolyte and lipid-like domains. Such an organization is only possible when the polycation PAH is confined between the rigid walls of the alkyl chains forming a stratified supramolecular array on each layer.

From the reflection positions, the lamella dimension (or repeat unit) has been determined to be 9.21, 8.61, 8.25, and 8.10 nm for $(DP/PAH)_1$, $(DP/PAH)_3$, $(DP/PAH)_5$, and $(DP/PAH)_7$, respectively. These results reveal that lamellar spacing decreases almost linearly upon increasing the number of DP/PAH bilayers. This implies that multilayers are more densely stacked when increases the number of layers in the film. This observation is in agreement with the fact that the sharpness of the Bragg peaks increases upon increasing the number of multilayers.

In close analogy with separated mesophase structures, the lamellar structure can be interpreted as consisting of sheets of thickness d_1 constituted of a non-ionic phase (hydrophobic moieties) and sheets of thickness d_2, constituted of a ionic phase (polyelectrolyte plus ionic head groups). The long period is given by $d = d_1 + d_2$. From the relative intensities of the lamellar reflections, the thickness of d_1 and d_2 for $(DP/PAH)_3$ and $(DP/PAH)_7$ multilayers were calculated to be 5.74 and 2.87 nm, and 6.07 and 2.03 nm, respectively. Interestingly, it is observed that the decrease in the lamellar spacing upon increasing the number of bilayers arises from the significant compaction of the polyelectrolyte layer rather than the reorganization of the lipid-like domains. Indeed, d_1 values obtained by XRR further corroborate that dodecylphosphate domains are assembled into the film forming a bilayer in a tail-to-tail arrangement.

Analysis of XRR data provides information regarding the coherent scattering length density (SLD) distribution normal to the sample surface, *i.e.*: z direction. X-ray SLD is proportional to the electron density and its profile across the multilayered film can be obtained by using a least-squares fitting routine. In our case, data were fitted using the StochFit 1.7 Package.[55] The SLD profiles obtained from the best fittings of the reflectivity profiles are shown in Fig. 3 as a function of distance (z) from the Si substrate, where the SLDs of PAH, and DP were estimated in relation to the silicon substrate. Average values were 16.4×10^{-6} A^{-2} for the PAH layer and 18.2×10^{-6} A^{-2} for the DP layer. The fitted SLD profiles corroborate that well-defined stratified arrays of DP/PAH bilayers can be obtained. The quality of layer ordering revealed by the spacing between polyelectrolyte and alkyl layers is manifested in local maxima and minima in the SLD profiles. The SLD of the polar domains containing the polyelectrolyte and phosphate head groups (local maxima) refer to regions of higher electron density as compared with alkyl-rich domains (local minima).[56]

LbL films grown on silicon substrates were then characterized by atomic force microscopy (AFM). Films display a flat morphology in the presence of some isolated grains, with a diameter in the 350–500 nm range (Fig. 4). The presence of these grains seems to be more evident in the case of $(DP/PAH)_2$ and $(DP/PAH)_4$ films. This observation is in agreement with XRR data indicating that thinner films are less organized and, according to AFM results, this fact could be ascribed to morphological effects.

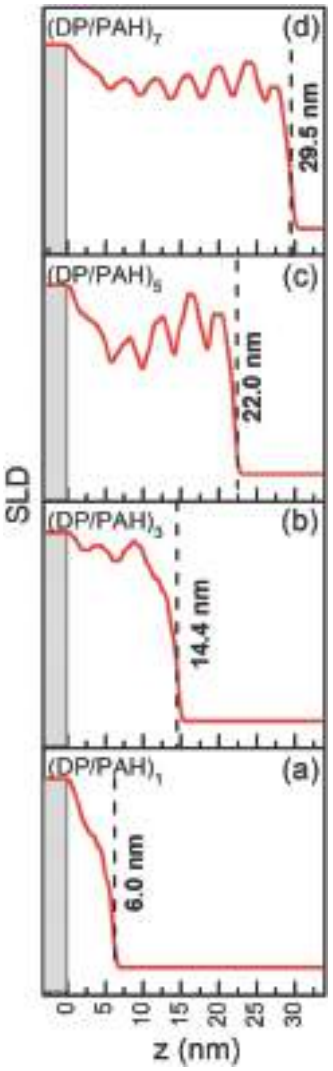

Fig. 3 Plot of the scattering length density (SLD) as a function of the profile depth in the z-direction obtained from XRR data of the self-assembled multilayers: (a) $(DP/PAH)_1$, (b) $(DP/PAH)_3$, (c) $(DP/PAH)_5$, (d) $(DP/PAH)_7$ multilayers.

It is also observed that the film morphology is not strongly influenced by the chemical nature of the capping layer, as confirmed in the recorded AFM height images. The contrast in the AFM phase images (see ESI† file for details, Fig. S1) does not provide evidence for the presence of patches, islands or phase-segregated domains,[57] pointing to a favorable interaction between PAH and DP units that leads to the uniform spreading of each layer during the assembly step.

In this sense, we should note that the assembly between PAH and DP in water is driven by both electrostatic and hydrophobic interactions.[58] As such, to characterize the prevalence of hydrophobicity as a driving force in the assembly process we carried out water contact angle measurements on multilayers capped with PAH and DP, respectively. Exposure of the multilayers to a drop of water reveals contact angles between 83° to 108° (see Table 1). These values reflect the hydrophobic character of the samples, showing a more hydrophobic behavior when DP is forming the outermost layer.

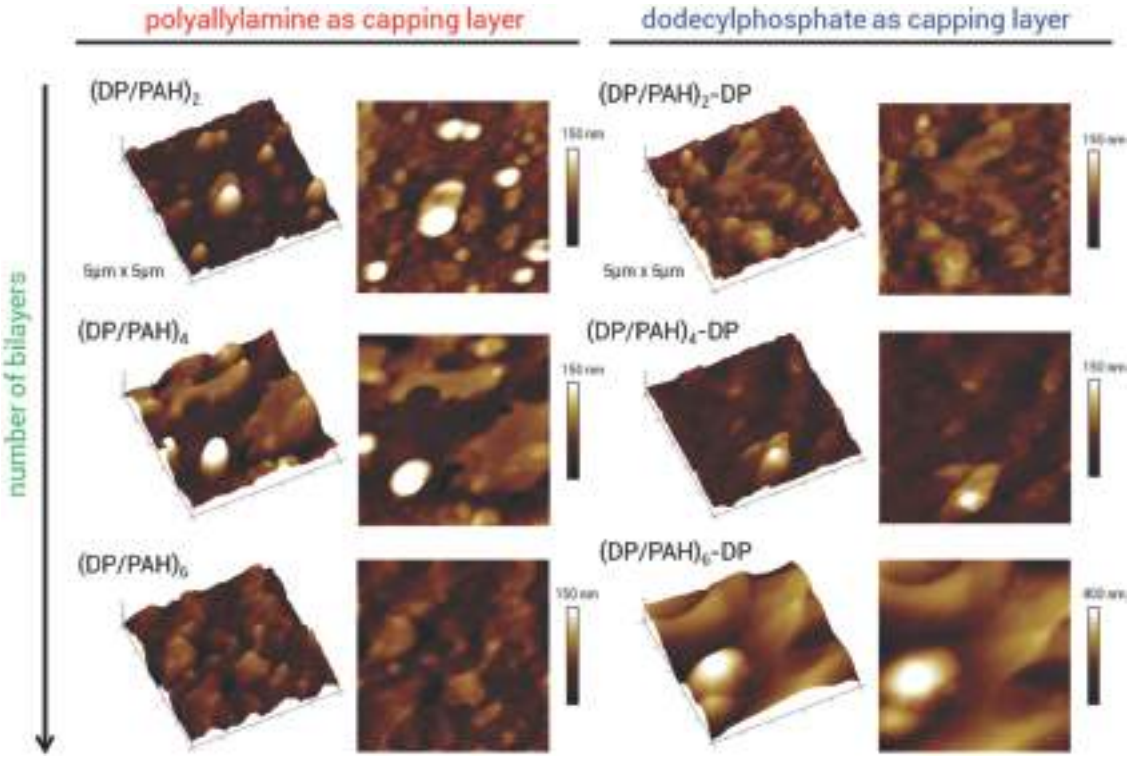

Fig. 4 Atomic force microscopy imaging (5 × 5 μm^2) of: (left) (DP–PAH)$_2$ (RMS roughness: 33.8 nm), (DP/PAH)$_4$ (RMS roughness: 30.2 nm), and (DP/PAH)$_6$ (RMS roughness: 17.6 nm); (right) (DP–PAH)$_2$–DP (RMS roughness: 25.9 nm), (DP/PAH)$_4$–DP (RMS roughness: 16 nm), and (DP/PAH)$_6$–DP (RMS roughness: 66.3 nm).

Table 1 Contact angle measurements corresponding to DP- and PAH-capped multilayers

	Average contact angle (°)	
No. of bilayer	DP	PAH
1	83.7	88.3
2	106.7	90.3
4	106.7	97.0
6	105.7	103.2
8	108.4	104.6

The increasing hydrophobicity of the surface upon adding more layers to the film supports the idea that the wetting characteristics are influenced by the presence of organized hydrophobic alkyl domains close to the film surface.

In principle, the anionic headgroups of the DP molecules bind to the cationic sites of the PAH layer, leaving the hydrophobic hydrocarbon tails exposed, which would increase the hydrophobicity of the PAH/DP outer layer. It is, however, noteworthy that PAH assembly on DP-capped surfaces also leads to hydrophobic surfaces (see Table 1). In close resemblance to DP-capped films, the hydrophobicity of PAH-capped films increases after incorporating successive layers to the multilayered film. In this regard, we should note that wetting measurements are very sensitive to the chemical nature of the outermost region of the films, ~3 nm. If we consider that the thickness of the assembled PAH layer is ~2 nm, the contact angle values might indicate that the underlaying alkyl chains of DP molecules dominate the wetting characteristics of the film and prevails on hydrophilic character of the PAH layer. A similar observation was reported in other works for the adsorption of sodium dodecyl sulfate (SDS) on poly(ethylenimine)[59] and poly(allylamine)[60] in multilayered thin films.

The chemical nature of the films was determined by X-ray photoelectron spectroscopy (XPS). Fig. 5 shows N1s and P2p core regions of the XPS spectra of a Si/PEI/(DP/PAH)$_5$ assembly. Quantitative results by fitting of the XPS data for assemblies of different number of bilayers are summarized in Table 2.

N1s XPS signal was resolved into two peaks, at binding energies corresponding to 401.8 eV and 399.3 eV (Fig. 5).[61,62] These peaks have been assigned to N–C species of protonated and neutral amines respectively.[63] From the relative area of these two contributions, the protonation degree was determined for PAH in each assembly. These results indicate that PAH is highly protonated (about 90%). These values of protonation degree are higher than those calculated at pH 8 using the reported pK_a for PAH in solution (8.5 [64]–9.2 [65]) and, recently, for adsorbed PAH (8.7 [66]), indicating that some additional protonation is induced by interaction with the DP components within the assemblies. The increase in the protonation degree of surface amino-groups by interaction with simple phosphate anions has been recently reported.[66] The P2p core region shows the spin–orbit coupling with binding energy positions at 133.7 for P2p$_{3/2}$ and 135.1 eV for P2p$_{1/2}$. The atomic N/P ratio

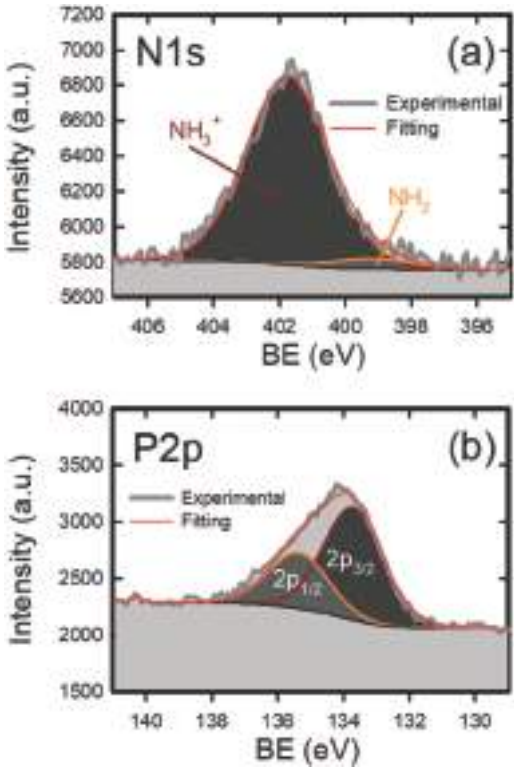

Fig. 5 XPS spectra (including fittings) of a $(DP/PAH)_5$ multilayer assembled on Si. The plots describe the binding energy region corresponding to (a) N1s and (b) P2p.

Table 2 Peak position and assignment of the components employed for fitting XPS results

	N1s components		
	NH_2	NH_3^+	Atomic ratio N/P
BE	399.3 eV	401.8 eV	
$Si/PEI/(DP/PAH)_1$	12%	88%	6.5
$Si/PEI/(DP/PAH)_3$	8%	92%	4.2
$Si/PEI/(DP/PAH)_5$	5%	95%	4.3
$Si/PEI/(DP/PAH)_8$	8%	92%	3.3

was determined for each assembly by employing the relative effective sections obtained from the XPS results of $(NH_4)_2HPO_4$. The values reported in Table 2 indicate that more than three amine groups per phosphate anion are present in the assemblies. The decrease in the proportion as the number of bilayers increases could be attributed to the influence of the initial PEI layer that also contributes to the N1s core signal (Table 2).

We might wonder about the possibility of intrinsic charge compensation within the films. Kooijman and co-workers have shown that the interaction with charged primary and quaternary amines induces a higher dissociation degree of phosphatidic acid, changing its electrostatic charge from −1 to −2 at neutral pH.[67–69] Even it has been recently shown that simple phosphates anions bound to amine surface groups present a higher dissociation degree as a consequence of the interaction with the positively charged groups.[66] Taking into account the pK_a values reported for dodecylphosphate (2.8 and 7.2)[70] and the putative effect of the charged amino groups, it could be reasonable to consider that phosphate groups are doubly charged within the assemblies. However, this charge is not enough to compensate the charge of amine moieties even for the thickest films. The presence of chloride (and the absence of Na), as revealed by the XPS (see ESI† file for details, Fig. S2), confirms the idea that the PAH layer contains some proportion of chloride anions from solution to compensate the excess of positive charge.

Self-assembled films were then characterized by Fourier transform infrared (FTIR) spectroscopy (see Table 3). Some characteristic bands of organic phosphates can be observed in the spectrum of solid DP (Fig. 6). The bands at about 950 cm^{-1} are due to P–OH stretching modes whereas the bands at about 1075 cm^{-1} has been assigned to P–O stretching modes in POC groups.[71] the bands at about 1150–1250 cm^{-1} are assigned to P═O stretching.[72] There are also other bands at 1100–1190 cm^{-1}, assigned to C–C and C–O stretching, and the intense band at 1470 cm^{-1} has been assigned to the HCH scissoring modes.[73]

The FTIR spectrum of PAH drop-casted on Si from an acidic solution is also presented in Fig. 6. In this wavelength range, PAH shows two main bands separated by about 100 cm^{-1}. These peaks have been assigned to bending modes of protonated amine groups.[74,75] In the present case, they appear at 1507 and 1610 cm^{-1} and correspond to symmetric and antisymmetric bending modes of the protonated primary amines respectively.[76,77] There is also a band at about 1460 assigned to CH bending modes.[78]

The main bands from PAH and DP are also present in the spectrum of the LbL assembly (Fig. 6). However, there are some

Table 3 Vibrational spectroscopic data of DP/PAH assemblies

Bands	Position	Assignments
(1)	950 cm^{-1}	P–OH stretching
(2)	1075 cm^{-1}	P–O stretching
(3)	1150–1250 cm^{-1}	P═O stretching
(4)	1507/1541 cm^{-1}	N–H bending
(5)	1610/1634 cm^{-1}	N–H bending

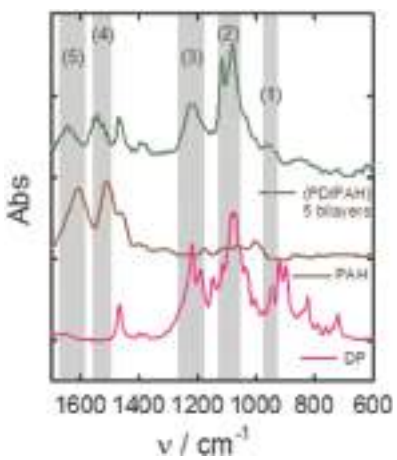

Fig. 6 FTIR spectra of solid DP, PAH and a $(DP/PAH)_5$ assembly deposited on a Si substrate.

features that indicate the interaction of the protonated amine groups and phosphates within the assemblies. Firstly, the band at about 950 cm^{-1} has almost disappeared, which indicates a higher dissociation of the POH groups as could be expected from the association to $-NH_3^+$ moieties.[66] Moreover, the peaks assigned to phosphate are broader, indicating a less defined structure compared with that in the solid DP. On the other hand, those bands assigned to the bending modes of ammonium groups shift to higher wavenumbers. This type of shift has been ascribed to the interaction with negative species,[79,80] supporting the idea of the association to anionic phosphates.

Assembly and compartmentalization of redox units in highly organized stacked multilayers

One of the attractive features of the layer-by-layer technique is its ability to create complex interfacial architectures with a high level of hierarchy and separate compartments. In this sense, compartmentalization and positional assembly are two essential and complementary requisites involved in biological systems to control concerted process. Material scientists have fruitfully employed these notions to build diverse classes of hierarchically structured solids and thin-films using many different building blocks including crystallizing molecules,[81] colloids,[82] mesoporous architectures,[83] or phase-separating polymers,[84] among others. Here, we extend this notion to create mesoscale-organized interfacial architectures displaying well-defined stratified phase-separated regions within the film that can behave as functional nanodomains, with highly controlled chemistry and interactions within restricted volumes. Our goal is the tailored production of complex film structures displaying spatially-addressed chemistry based on the control of assembly process. As is well-known the self-assembly of amphiphilic molecules in water represents a valuable strategy to create compartmentalized materials (*e.g.*, micelles, vesicles, and nanogels). In principle, the generation of microdomains within organized mesostructures would facilitate the introduction of different functional units into discrete but closely located nanospaces. The amphiphilic structure of surfactants and their aggregating properties in aqueous solutions provide a multifunctional environment for the solubilization and partition of molecules whose water solubility is rather low.

With this idea in mind, we solubilized ferrocene (Fc) in dodecyl phosphate micelles with the aim of spatially-addressing redox-active units in the hydrophobic domains of the multilayered films. Ferrocene is a highly hydrophobic compound – only sparingly soluble in water – that can be solubilized in aqueous solutions through the encapsulation in surfactant micelles without detrimental effects on its intrinsic redox activity.

Multilayer films exhibiting compartmentalized redox-active domains (Scheme 2) were fabricated by alternating deposition of polyallylamine (PAH) and ferrocene-loaded dodecyl phosphate micelles on Si substrates. The presence of ferrocene within the assemblies was confirmed by XPS. The appearance of the signal assigned to the Fe2p core level in the XPS spectrum of the $Si/PEI/(DP/PAH)_5$ assembly prepared from a solution of DP saturated with ferrocene (Fig. 7) clearly indicates that ferrocene in effectively incorporated into the films. The binding energy (BE) of the $Fe2p_{1/2}$ and $Fe2p_{3/2}$ components were 723.8 and 710.5 eV respectively, which is consistent with the presence of ferrocene moieties.[85,86]

Concomitantly, XRR characterization confirmed that the presence of ferrocene in the multilayer does not alter the internal organization of the stratified LbL films, as indicated by the presence of well-defined Bragg peaks (Fig. 8). From the reflectivity data we can conclude that the Fc is incorporated into well-stratified multilayers exhibiting highly oriented lamellar organization. Considering the hydrophobic nature of Fc we infer that the redox units are located in the hyrophobic alkyl domains. For instance, the slight shift in the position of q^* indicates that the lamellar spacing changes from 4.2 to 4.4 nm due to the steric contribution of Fc molecules located in the hydrophobic domains.

On the other hand, the presence of distinct, periodic, and sharply contrasting PAH and DP layers in the fitted SLD profile

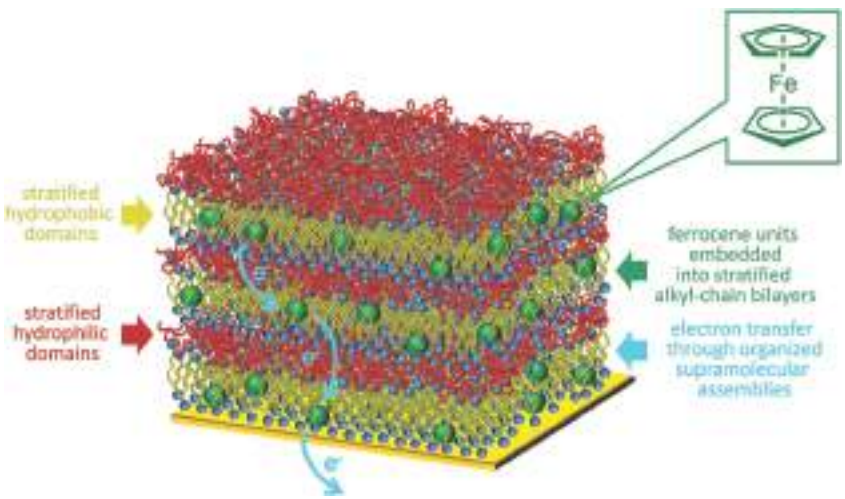

Scheme 2 Schematic representation of the LbL-assembled supramolecular stratified structure integrating ferrocene units in the stratified hydrophobic domains.

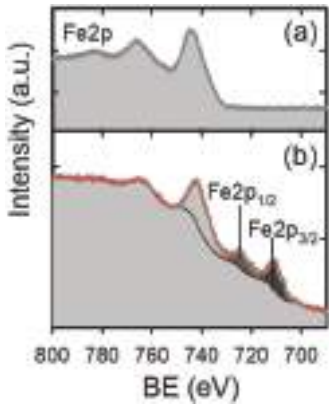

Fig. 7 XPS spectra in the Fe2p region for a Si/PEI/(DP/PAH)$_5$ assembly prepared without (a) and with (b) ferrocene in the DP solution.

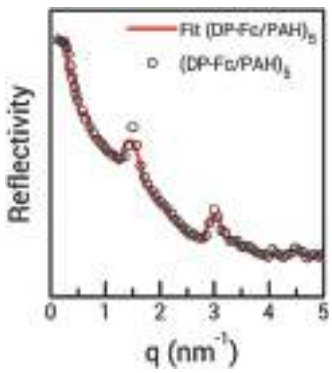

Fig. 8 Specular X-ray reflectivity curve (empty circles) together with a fit to the data (solid red line) corresponding to a (DP-Fc/PAH)$_5$ supramolecular stratified assembly integrating ferrocene (Fc) into the stratified domains. The X-ray structural data corroborates the formation of a stratified structure even in the presence of ferrocene hosted in the multilayer.

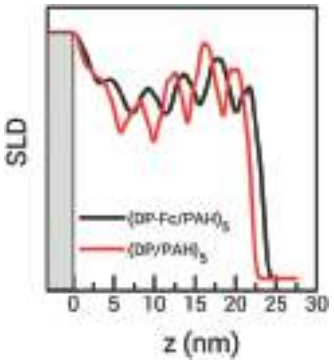

Fig. 9 Plot of the scattering length density (SLD) as a function of the profile depth in the z-direction obtained from XRR data of the self-assembled multilayers in the absence (red trace) and in the presence of ferrocene (Fc) units hosted in the multilayer. The XRR-derived data corroborate that the presence of Fc induces slight dimensional changes without affecting the stratified nano-organization of the supramolecular assembly.

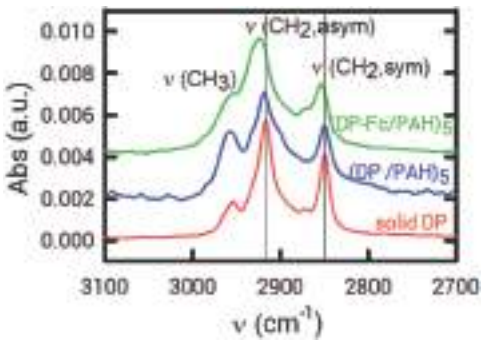

Fig. 10 ATR-FTIR spectra in the region of C–H stretching. For the sake of clarity, spectra were shifted in absorbance.

is striking (Fig. 9), further indicating that layering is preserved in the presence of Fc. It should be noted that SLD contrast between polar (higher electron density) and non-polar (lower electron density) domains is slightly decreased due to the insertion of electron-rich Fc units in the alkyl bilayers.

We have so far demonstrated that the presence of Fc does not alter the nanoscale lamellar organization of the stratified film. Now, we will study the influence of the Fc units (guest molecules) on the molecular organization of the hydrophobic alkyl domains. ATR-FTIR spectra of the DP/PAH assembly and solid DP are presented in Fig. 10. The bands at about 2850 and 2920 cm^{-1} are assigned to symmetric and asymmetric stretching modes of methylenes and the band at 2950 cm^{-1} is assigned to C–H stretching modes of methyl groups. The bands of the methylene stretching have been extensively employed as markers of the degree of order of the packing of aliphatic chains.[87,88] Both, the shifting to higher wavenumbers as well as the broadening of these bands have been associated to an increase in the disorder and a higher population of *gauche* conformations.[89] Moreover, the increase in the intensity ratio (I_{asym}/I_{sym}) is related to the increase in the disorder of the chains.[90] In the present case, the band positions of the methylene stretching and the intensity ratio reveals that the packing of the aliphatic chains of DP in the assemblies is similar to that in the solid (refer to ESI† file for further details, Table S1). The ATR-FTIR spectrum of a DP-Fc/PAH assembly is also presented in Fig. 10 for comparison. In this case, the features of the methylene bands clearly indicate a higher disorder of the aliphatic chains, which suggest that the Fc moieties are located within the DP domains and promote the local molecular disorder of the hydrophobic domains.

The insertion of electroactive Fc units into the multilayered films was also proven by cyclic voltammetry. Fig. 11 shows the cyclic voltammetry (CV) of (DP-Fc/PAH)$_5$ film, which exhibits a highly reversible electrochemical response. The formal potential of Fc units embedded into the alkyl domains of the stratified multilayer was 0.28 V (*versus* Ag/AgCl). In this regard, Creager and Rowe[91] demonstrated that the formal potential of Fc can be strongly influenced by the nature of the interfacial microenvironment. These authors showed that embedding an electroactive moiety in an alkyl pocket could affect the redox reaction by preferentially stabilizing one form of the redox couple relative to another (a solvent effect), or by preventing counterions in solution

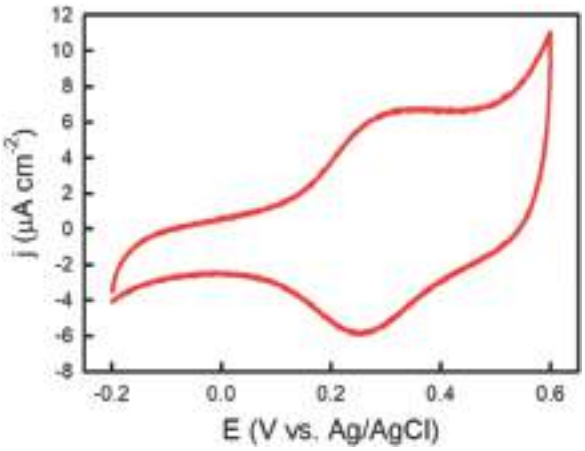

Fig. 11 Cyclic voltammogram of a $(DP\text{-}Fc/PAH)_5$ film assembled on a gold electrode. Scan rate: 100 mV s^{-1}. Electrolyte: 0.1 M KCl.

from entering the pocket (a double-layer effect). Both of these effects could cause the apparent formal potential for the immobilized redox species to shift. In our case, even though the measured values fall into the typical range of ferrocene, the rather low formal potential reflects that Fc units are embedded into the alkyl bilayer but in close proximity to the polar environment provided by the polyelectrolyte-rich domains. We hypothesize that the disorder induced by the incorporation of ferrocene in the lipid layer might promote the transport of co-ions and counterions during the electrochemical cycling, thus facilitating the reversible redox reaction of the ferrocene units.

In addition, we should also note that despite the fact that redox units are not covalently attached to the film, the electroactive response is very stable over time. Continuous cycling of Fc-containing stratified (DP/PAH) multilayers at a scan rate of 50 mV s^{-1} during several hours revealed no evidence of material loss or decrease in electroactivity. Thus, we can conclude that the Fc units remain robustly inserted into the stratified domains within the experimental potential range. This is a remarkable feature if we consider that in many cases redox-active multilayers held together solely by electrostatic interactions material losses after extensive redox activity.[92]

Construction of stratified, enzyme-containing multilayer assemblies – bioelectrochemical nanoarchitectonics

Multilayer films were fabricated by alternating deposition of redox-active osmium complex tagged poly(allylamine) hydrochloride (OsPA), sodium dodecylphosphate (DP) and glucose oxidase (GOx). The protocol leading to the layer-by-layer formation of multicomposite molecular assemblies comprised of OsPA/DP/OsPA/GOx multilayers is schematically outlined in Scheme 3. The reason for incorporating an additional OsPA layer in between the surfactant bilayer and the GOx layer is that this configuration improves the "wiring" efficiency of the redox assembly. Alternating

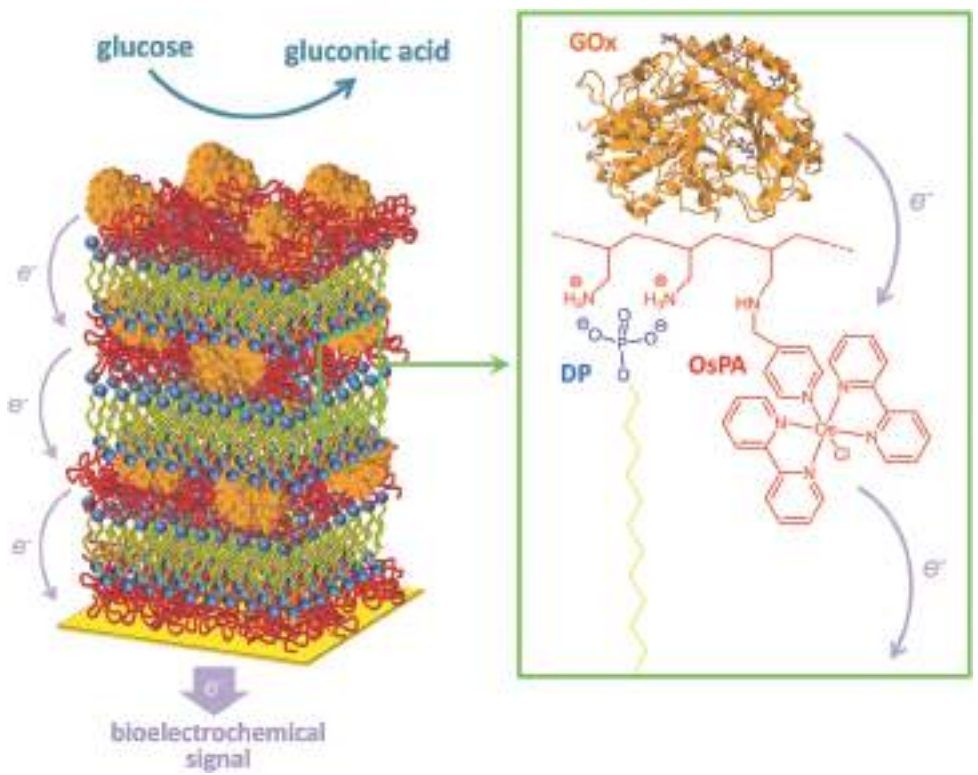

Scheme 3 Simplified schematic of the glucose-responsive ternary supramolecular assembly. Poly(allylamine) containing an osmium polypyridil complex (OsPA), dodecylphosphate (DP) and glucose oxidase (GOx) are sequentially assembled in a layer-by-layer fashion onto the electrode surface. The figure displays the constituting building blocks (not to scale) participating in the generation of the bioelectrochemical signal in the presence of glucose as well as a simplified view of the stratified organization of the interfacial architecture.

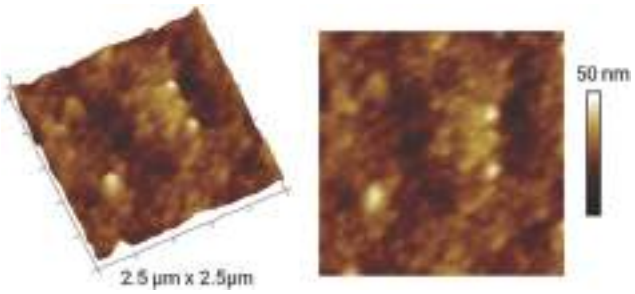

Fig. 12 Atomic force microscopy imaging (5 × 5 mm^2) (3D and top view) corresponding to (OsPA/DP/OsPA/GOx)$_5$ films LbL-assembled on silicon.

layers of OsPA, DP and GOx were then deposited using solutions with concentrations, 0.4% w/v, 10 mM and 1 mg ml^{-1}, respectively. In this case, we have diluted the concentration of dodecyl phosphate to avoid surfactant-induced denaturation of the enzyme.[93]

Representative AFM images of the morphology of the enzyme-containing stratified films are shown in Fig. 12. (OsPA/DP/OsPA/GOx)$_5$ films grown on silicon consist of tightly packed grains leading to the formation of a homogenously distributed nodular-like film. Concomitantly, a quantitative structural analysis of the multilayer thin films deposited on substrates in the out-of-plane and in-plane directions of the film was carried out by using grazing-incidence small-angle X-ray scattering (GISAXS). Indeed, the presence of lamellar structures may be checked using GISAXS measurements, which are sensitive to variations in structure in the plane of the sample.

GISAXS characterization of (OsPA/DP/OsPA/GOx)$_5$ films are shown in Fig. 13a. The GISAXS patterns eloquently reveals the presence of meso-organization arising from the lamellar domains oriented parallel to the substrate. Both patterns show a bright region (highest intensity) in the direction q_z (for $q_y \rightarrow 0$) and the presence of a faint halo (Fig. 13a). This suggests that while the lamellar domains are predominantly oriented parallel to the substrate there is some contribution of randomly oriented small domains.

The position of the scattering maxima with respect to the q_z axis, the scattering wave vector perpendicular to the surface of the film, corresponds to the lamellar organization of hydrophilic and hydrophobic domains pores. The q_y value of 2.09 nm^{-1}, at scattering maxima, corresponds to the average lamellar spacing of 3 nm in the z-direction perpendicular to the film surface.

Taking into account that bioelectrochemical nanoarchitectonics is the main application of this nanostructured system, we considered that an aqueous environment represents a more realistic scenario for studying the nano- and mesoscale organization of the multilayered film. As is well known water uptake may lead to swelling of hydrophilic polyelectrolyte domains in phase-segregated materials.[94,95]

With this in mind, we performed GISAXS experiments under high humidity conditions (relative humidity, RH ~ 95%). We observed a slight increase in lamellar spacing (l) from 3.0 to 3.4 nm upon increasing the relative humidity from 1 to 95%

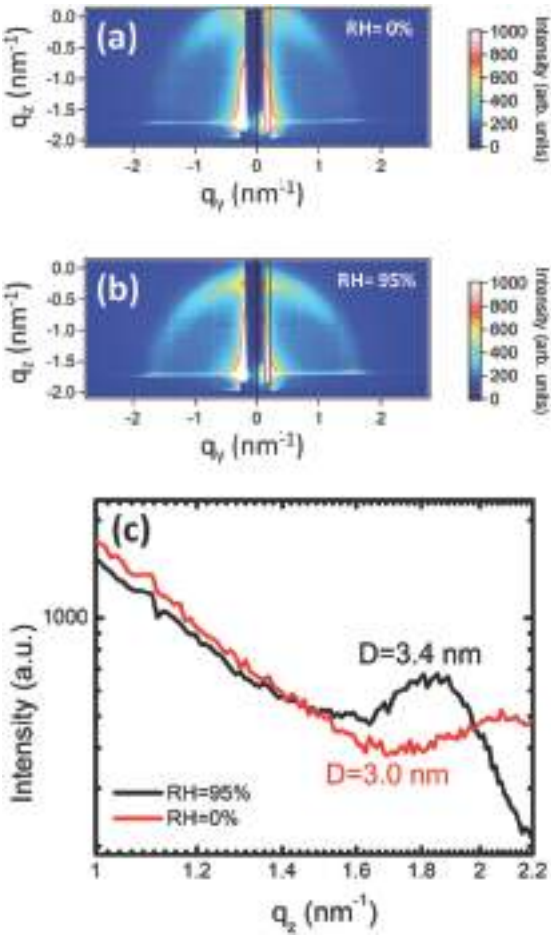

Fig. 13 GISAXS patterns corresponding to a (OsPA/DP/OsPA/GOx)$_5$ multilayer self-assembled on a silicon substrate measured at: (a) RH ~ 0% and (b) RH ~ 95%. (c) Out-of-plane scattering profiles extracted along the q_z direction (at q_y = 0.2 nm^{-1} with Δq_z width corresponding to ±0.01 nm^{-1}) from the GISAXS patterns of (OsPA/DP/OsPA/GOx)$_5$ multilayers obtained under different humidity conditions. GISAXS data confirm that the presence of water promotes the swelling of the supramolecular assembly without affecting the stratified organization.

(Fig. 13b). In few words, the lamellar domains experience only slight dimensional changes (13%) in the presence of water. These results confirm the non trivial fact that the stratified organization in which the polyelectrolyte bearing redox centers, the enzymes and the alkyl chains accommodate during the multilayer growth is preserved after immersion in water.

Once demonstrated that the stratified meso-organization the multilayer is not altered by the aqueous environment we proceeded to characterize the bioelectrocatalytic features of stratified enzyme-containing assemblies in the presence of the enzyme substrate.

Fig. 14 shows the CVs of a gold electrode modified with (OsPA/DP/OsPA/GOx)$_5$ multilayers in the absence and presence of 50 mM glucose. When no glucose was present, a reversible redox peak was observed at 370 mV. However, upon addition of glucose, there was a substantial increase in the oxidation current and a concomitant decrease in the reduction current. This behavior is indicative of the redox polymer mediation of the well-known GOx-catalyzed oxidation of glucose.

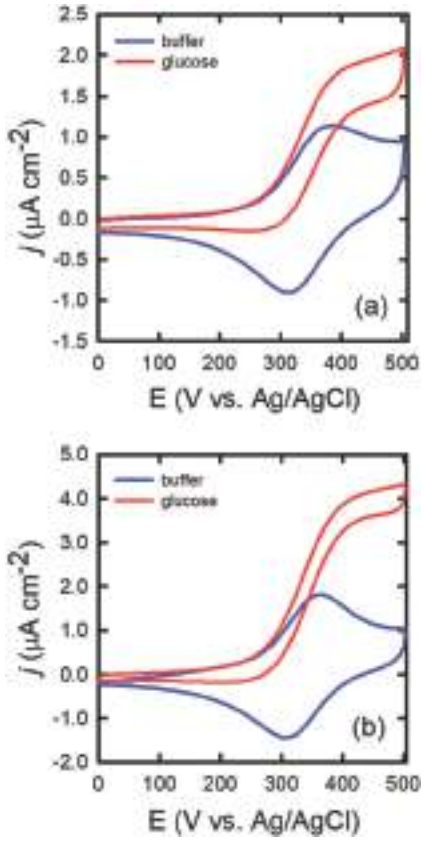

Fig. 14 Cyclic voltammograms corresponding to: (a) (OsPA/DP/OsPA/GOx)$_5$ and (b) (OsPA/DP/OsPA/GOx)$_5$/OsPA. The blue trace refers to voltammetric measurements performed in the absence of glucose whereas the red trace refers voltammetric measurements performed in the presence of 50 mM glucose. Supporting electrolyte: 100 mM Tris–HCl buffer +0.1 M NaCl (pH 7.4).

The voltammetric response eloquently illustrates the responsiveness of the GOx-containing supramolecular assembly to the presence of the glucose in the electrolyte solution. Indeed, the stacked multilayers constituted of (OsPA/DP/OsPA/GOx)$_5$ reveal a significant anodic current implying that glucose is readily oxidized by the enzyme-containing mesostructured redox-active assembly. Note, however, that the "wiring" efficiency is lower than in the case of less-organized, gel-like multilayer asemblies (see Fig. S3 in ESI† file for a direct comparison between the electrochemical behaviour of highly stratified (OsPA/DP/OsPA/GOx)$_5$ and amorphous-like (OsPA/GOx)$_5$ multilayers).

This being said, we should note that the goal of our work was not to demonstrate that the stratification improves the "wiring", but instead, that the redox "wiring" followed by bioelectrocatalytic activity can be attained in highly stratified multilayers – a fact that has not been discussed or demonstrated previously.

Conclusions

Structural control of highly-ordered multilayers displaying spatially-addressed functional domains is a fundamental ambition of supramolecular assembly research in solution-based systems. Herein, we have proposed a novel and facile pathway for growing highly oriented multilayers based on the assembly of a polycation, PAH, and an anionic surfactant, DP, that ultimately act as structure directing agent.

We have shown that highly stratified films may be obtained, consisting of a regular lamellar nanostructure extending over the films, with preferential orientation parallel to the substrate. This feature is different from that of the conventional polycation–polyanion and protein–polyion multilayer assemblies which display a "fuzzy" organization with no internal structure. The presence of the surfactant forming organized mesophases is conducive to stratified multilayers of higher order. However, this condition is not sufficient, if we consider that previous reports describing the multilayer assembly of surfactant micelles and polyelectrolytes did not lead to the formation highly stratified systems. We hypothesize that the strong electrostatic and ion pairing interaction between amino groups of PAH and phosphate groups of DP – together with the hydrophobic forces introduced by alkyl chains – are responsible for the formation of ordered surfactant bilayers during the assembly process. Eventually, these bilayers act as physical barriers that hinder interdifussion of the polyelectrolye chains and confer dimensional stability to the nanoarchitectured multilayer system. As a result, this strategy constitutes a rapid and experimentally very simple technique to create complex stratified multilayers with precise control of layer composition and thickness. The versatility of the present methodology is remarkable as the deposition process allowed for excellent spatial segregation of individual components in nanocompartmentalized stratified domains. As a way of example, the stratified multilayers containing hydrophobic and hydrophilic domains were successfully employed as hosts for redox-active units and bioactive elements and used to construct electrochemical interfaces. Ferrocene molecules were hosted into the lipophilic nanocompartments leading to the site-selective location of redox-active units into the stratified assembly. Then, glucose oxidase was selectively embedded into the hydrophilic nanocompartments originated from the spatial segregation polyallylamine bearing Os-based redox centers. Bioelectrocatalysis in the presence of glucose was shown to occur in ordered, stratified multilayers as evidenced by generation of well-defined amperometric signals. Examples described here were applied specifically to electrochemical "nanoarchitectonics". However, the possibility to fabricate functional, well-stratified multilayers using this strategy reaches beyond this particular field.

Taken altogether, this approach offers a complete set of tools allowing complex stratified interfacial architectures to be fabricated that can serve as nanocompartments for spatial confinement of small functional molecules, or even functional polymers and biomolecules. We believe that the proposed methodology can further expand the reach and scope of nanoarchitectonics provided that it has been demonstrated that multilayer assembly in the presence of structure-directing agents is a valuable tool for structural control of functional stratified nanosystems. As such, we consider that this strategy in the toolkit of rational layer-by-layer

assembly will contribute to the rapid development of complex functional multilayered 3D-nanoarchitectures exhibiting high degree of stratification.

Conflicts of interest

There are no conflicts to declare.

Acknowledgements

The authors acknowledge financial support from CONICET (PIP0370), ANPCyT (PICT-2013-0905, PICT-2014-3792, PICT-2016-1680), Fundación Petruzza and the Austrian Institute of Technology GmbH (AIT–CONICET Partner Lab: ''Exploratory Research for Advanced Technologies in Supramolecular Materials Science'' – Exp. 4947/11, Res. No. 3911). A. L. acknowledges CONICET for a doctoral fellowship. M. C. and O. A. gratefully acknowledge the Laboratório Nacional de Luz Síncrotron (LNLS, Campinas – Brazil) for financial support and granting access to synchrotron facilities (XRD2 – 13391; XRD2 – 11639 and XRD2 – 14358). M. L. C., W. A. M., C. v. B., E. M., L. I. P., F. B., M. C. and O. A. are CONICET fellows.

References

1 G. Decher and J. B. Schlenoff, *Multilayer Thin Films*, John Wiley & Sons, 2002, pp. 1–46.
2 X. Shi, M. Shen and H. Mohwald, *Prog. Polym. Sci.*, 2004, **29**, 987–1019.
3 K. Ariga, Q. Ji, J. P. Hill and A. Vinu, *Soft Matter*, 2009, **5**, 3562.
4 K. Ariga, J. P. Hill and Q. Ji, *Phys. Chem. Chem. Phys.*, 2007, **9**, 2319.
5 P. Bertrand, A. Jonas, A. Laschewsky and R. Legras, *Macromol. Rapid Commun.*, 2000, **21**, 319–348.
6 F.-X. Xiao, M. Pagliaro, Y.-J. Xu and B. Liu, *Chem. Soc. Rev.*, 2016, **45**, 3088–3121.
7 Y. Lvov, F. Essler and G. Decher, *J. Phys. Chem.*, 1993, **97**, 13773–13777.
8 I. Ichinose, K. Fujiyoshi, S. Mizuki, Y. Lvov and T. Kunitake, *Chem. Lett.*, 1996, 257–258.
9 H. Lee, L. J. Kepley, H. G. Hong and T. E. Mallouk, *J. Am. Chem. Soc.*, 1988, **110**, 618–620.
10 M. Aono, Y. Bando and K. Ariga, *Adv. Mater.*, 2012, **24**, 150–151.
11 K. Ariga, M. V. Lee, T. Mori, X.-Y. Yu and J. P. Hill, *Adv. Colloid Interface Sci.*, 2010, **154**, 20–29.
12 M. Ramanathan, L. K. Shrestha, T. Mori, Q. Ji, J. P. Hill and K. Ariga, *Phys. Chem. Chem. Phys.*, 2013, **15**, 10580.
13 A. H. Khan, S. Ghosh, B. Pradhan, A. Dalui, L. K. Shrestha, S. Acharya and K. Ariga, *Bull. Chem. Soc. Jpn.*, 2017, **90**, 627–648.
14 K. Ariga, V. Malgras, Q. Ji, M. B. Zakaria and Y. Yamauchi, *Coord. Chem. Rev.*, 2016, **320–321**, 139–152.
15 K. Ariga, A. Vinu, Y. Yamauchi, Q. Ji and J. P. Hill, *Bull. Chem. Soc. Jpn.*, 2012, **85**, 1–32.
16 K. Ariga, Y. Yamauchi, G. Rydzek, Q. Ji, Y. Yonamine, K. C.-W. Wu and J. P. Hill, *Chem. Lett.*, 2014, **43**, 36–68.
17 J. Wang, J. Tang, B. Ding, V. Malgras, Z. Chang, X. Hao, Y. Wang, H. Dou, X. Zhang and Y. Yamauchi, *Nat. Commun.*, 2017, **8**, 15717.
18 K. Glinel, A. Laschewsky and A. M. Jonas, *J. Phys. Chem. B*, 2002, **106**, 11246–11252.
19 X. Arys, A. Laschewsky and A. M. Jonas, *Macromolecules*, 2001, **34**, 3318–3330.
20 E. R. Kleinfeld and G. S. Ferguson, *Science*, 1994, **265**, 370–373.
21 N. A. Kotov, T. Haraszti, L. Turi, G. Zavala, R. E. Geer, I. Dékány and J. H. Fendler, *J. Am. Chem. Soc.*, 1997, **119**, 6821–6832.
22 D. M. Kaschak and T. E. Mallouk, *J. Am. Chem. Soc.*, 1996, **118**, 4222–4223.
23 T. Sasaki, Y. Ebina, M. Watanabe and G. Decher, *Chem. Commun.*, 2000, 2163–2164.
24 T. Sasaki, Y. Ebina, T. Tanaka, M. Harada, M. Watanabe and G. Decher, *Chem. Mater.*, 2001, **13**, 4661–4667.
25 K. Glinel, A. Laschewsky and A. M. Jonas, *Macromolecules*, 2001, **34**, 5267–5274.
26 J. Cho, K. Char, J.-D. Hong and K.-B. Lee, *Adv. Mater.*, 2001, **13**, 1076–1078.
27 B. Yuan, L.-L. Xing, Y.-D. Zhang, Y. Lu, Z.-H. Mai and M. Li, *J. Am. Chem. Soc.*, 2007, **129**, 11332–11333.
28 B. Jean, F. Dubreuil, L. Heux and F. Cousin, *Langmuir*, 2008, **24**, 3452–3458.
29 M. Kiel, S. Mitzscherling, W. Leitenberger, S. Santer, B. Tiersch, T. K. Sievers, H. Möhwald and M. Bargheer, *Langmuir*, 2010, **26**, 18499–18502.
30 E. Kharlampieva, V. Kozlovskaya, J. Chan, J. F. Ankner and V. V. Tsukruk, *Langmuir*, 2009, **25**, 14017–14024.
31 O. Félix, Z. Zheng, F. Cousin and G. Decher, *C. R. Chim.*, 2009, **12**, 225–234.
32 J. J. Richardson, M. Bjornmalm and F. Caruso, *Science*, 2015, **348**, aaa2491.
33 D. M. Kaschak, J. T. Lean, C. C. Waraksa, G. B. Saupe, H. Usami and T. E. Mallouk, *J. Am. Chem. Soc.*, 1999, **121**, 3435–3445.
34 K. Glinel, A. M. Jonas, A. Laschewsky and P. Y. Vuillaume, *Multilayer Thin Films*, Wiley-VCH, Weinheim, 2003, pp. 177–205.
35 K. C. Wood, H. F. Chuang, R. D. Batten, D. M. Lynn and P. T. Hammond, *Proc. Natl. Acad. Sci. U. S. A.*, 2006, **103**, 10207–10212.
36 S. Peralta, J.-L. Habib-Jiwan and A. M. Jonas, *ChemPhysChem*, 2009, **10**, 137–143.
37 S. Lee, B. Lee, B. J. Kim, J. Park, M. Yoo, W. K. Bae, K. Char, C. J. Hawker, J. Bang and J. Cho, *J. Am. Chem. Soc.*, 2009, **131**, 2579–2587.
38 M. Kopeć, A. Rozpędzik, Ł. Łapok, T. Geue, A. Laschewsky and S. Zapotoczny, *Chem. Mater.*, 2016, **28**, 2219–2228.
39 J. Cho, J. Hong, K. Char and F. Caruso, *J. Am. Chem. Soc.*, 2006, **128**, 9935–9942.

40 K. Sakai, G. B. Webber, C.-D. Vo, E. J. Wanless, M. Vamvakaki, V. Bütün, S. P. Armes and S. Biggs, *Langmuir*, 2008, **24**, 116–123.
41 B. Qi, X. Tong and Y. Zhao, *Macromolecules*, 2006, **39**, 5714–5719.
42 Q. Bo, X. Tong, Y. Zhao and Y. Zhao, *Macromolecules*, 2008, **41**, 3562–3570.
43 N. Ma, H. Zhang, B. Song, Z. Wang and X. Zhang, *Chem. Mater.*, 2005, **17**, 5065–5069.
44 F. Lisdat, R. Dronov, H. Möhwald, F. W. Scheller and D. G. Kurth, *Chem. Commun.*, 2009, 274–283.
45 R. Dronov, D. G. Kurth, H. Möhwald, F. W. Scheller and F. Lisdat, *Angew. Chem., Int. Ed.*, 2008, **47**, 3000–3003.
46 R. Dronov, D. G. Kurth, H. Möhwald, R. Spricigo, S. Leimkühler, U. Wollenberger, K. V. Rajagopalan, F. W. Scheller and F. Lisdat, *J. Am. Chem. Soc.*, 2008, **130**, 1122–1123.
47 A. Mulder, J. Huskens and D. N. Reinhoudt, *Org. Biomol. Chem.*, 2004, **2**, 3409.
48 O. Crespo-Biel, B. Dordi, D. N. Reinhoudt and J. Huskens, *J. Am. Chem. Soc.*, 2005, **127**, 7594–7600.
49 O. Crespo-Biel, B. J. Ravoo, D. N. Reinhoudt and J. Huskens, *J. Mater. Chem.*, 2006, **16**, 3997.
50 G. R. Heath, M. Li, H. Rong, V. Radu, S. Frielingsdorf, O. Lenz, J. N. Butt and L. J. C. Jeuken, *Adv. Funct. Mater.*, 2017, **27**, 1606265.
51 D. V. Volodkin, P. Schaaf, H. Mohwald, J.-C. Voegel and V. Ball, *Soft Matter*, 2009, **5**, 1394.
52 D. Volodkin, Y. Arntz, P. Schaaf, H. Moehwald, J.-C. Voegel and V. Ball, *Soft Matter*, 2008, **4**, 122–130.
53 M. Michel, D. Vautier, J.-C. Voegel, P. Schaaf and V. Ball, *Langmuir*, 2004, **20**, 4835–4839.
54 R. Ma and T. Sasaki, *Annu. Rev. Mater. Res.*, 2015, **45**, 111–127.
55 S. M. Danauskas, D. Li, M. Meron, B. Lin and K. Y. C. Lee, *J. Appl. Crystallogr.*, 2008, **41**, 1187–1193.
56 T. Schubert, P. C. Seitz, E. Schneck, M. Nakamura, M. Shibakami, S. S. Funari, O. Konovalov and M. Tanaka, *J. Phys. Chem. B*, 2008, **112**, 10041–10044.
57 L. Sardone, C. C. Williams, H. L. Anderson, G. Marletta, F. Cacialli and P. Samorì, *Adv. Funct. Mater.*, 2007, **17**, 927–932.
58 C. D. Bain, P. M. Claesson, D. Langevin, R. Meszaros, T. Nylander, C. Stubenrauch, S. Titmuss and R. von Klitzing, *Adv. Colloid Interface Sci.*, 2010, **155**, 32–49.
59 M. S. Johal, B. H. Ozer, J. L. Casson, A. S. John, J. M. Robinson and H.-L. Wang, *Langmuir*, 2004, **20**, 2792–2796.
60 M. L. Cortez, A. L. Cukierman and F. Battaglini, *Electrochem. Commun.*, 2009, **11**, 990–993.
61 X. Song, Y. Ma, C. Wang, P. M. Dietrich, W. E. S. Unger and Y. Luo, *J. Phys. Chem. C*, 2012, **116**, 12649–12654.
62 J. E. Baio, T. Weidner, J. Brison, D. J. Graham, L. J. Gamble and D. G. Castner, *J. Electron Spectrosc. Relat. Phenom.*, 2009, **172**, 2–8.
63 N. Graf, E. Yegen, T. Gross, A. Lippitz, W. Weigel, S. Krakert, A. Terfort and W. E. S. Unger, *Surf. Sci.*, 2009, **603**, 2849–2860.
64 K. Itano, J. Choi and M. F. Rubner, *Macromolecules*, 2005, **38**, 3450–3460.
65 K. Lutz, C. Gröger, M. Sumper and E. Brunner, *Phys. Chem. Chem. Phys.*, 2005, **7**, 2812.
66 G. Laucirica, W. A. Marmisollé and O. Azzaroni, *Phys. Chem. Chem. Phys.*, 2017, **19**, 8612–8620.
67 E. E. Kooijman, D. P. Tieleman, C. Testerink, T. Munnik, D. T. S. Rijkers, K. N. J. Burger and B. de Kruijff, *J. Biol. Chem.*, 2007, **282**, 11356–11364.
68 E. E. Kooijman and K. N. J. Burger, *Biochim. Biophys. Acta, Mol. Cell Biol. Lipids*, 2009, **1791**, 881–888.
69 D. H. Mengistu, E. E. Kooijman and S. May, *Biochim. Biophys. Acta, Biomembr.*, 2011, **1808**, 1985–1992.
70 K. Nakayama, I. Tari, M. Sakai, Y. Murata and G. Sugihara, *J. Oleo Sci.*, 2004, **53**, 247–265.
71 J. O. Carnali and B. A. Pethica, *J. Phys. Chem. B*, 2006, **110**, 24936–24946.
72 I. Maege, E. Jaehne, A. Henke, H.-J. P. Adler, C. Bram, C. Jung and M. Stratmann, *Prog. Org. Coat.*, 1998, **34**, 1–12.
73 A. N. M. Carauta, V. de Souza, E. Hollauer and C. A. Téllez, *Spectrochim. Acta, Part A*, 2004, **60**, 41–51.
74 D. K. Kim, S. W. Han, C. H. Kim, J. D. Hong and K. Kim, *Thin Solid Films*, 1999, **350**, 153–160.
75 J. Choi and M. F. Rubner, *Macromolecules*, 2005, **38**, 116–124.
76 G. Lawrie, I. Keen, B. Drew, A. Chandler-Temple, L. Rintoul, P. Fredericks and L. Grøndahl, *Biomacromolecules*, 2007, **8**, 2533–2541.
77 B. G. Mathapa and V. N. Paunov, *Soft Matter*, 2013, **9**, 4780.
78 V. Zucolotto, M. Ferreira, M. R. Cordeiro, C. J. L. Constantino, D. T. Balogh, A. R. Zanatta, W. C. Moreira and O. N. Oliveira, *J. Phys. Chem. B*, 2003, **107**, 3733–3737.
79 W. A. Marmisollé, J. Irigoyen, D. Gregurec, S. Moya and O. Azzaroni, *Adv. Funct. Mater.*, 2015, **25**, 4144–4152.
80 R. A. Rajadhyaksha and H. Knözinger, *Appl. Catal.*, 1989, **51**, 81–92.
81 J. Aizenberg, A. J. Black and G. M. Whitesides, *Nature*, 1999, **398**, 495–498.
82 A. Van Blaaderen, R. Ruel and P. Wiltzius, *Nature*, 1997, **385**, 321–324.
83 Y. Huang, Y. Lin, X. Ran, J. Ren and X. Qu, *Chem. – Eur. J.*, 2016, **22**, 5705–5711.
84 J. Boekhoven, P. van Rijn, A. M. Brizard, M. C. A. Stuart and J. H. van Esch, *Chem. Commun.*, 2010, **46**, 3490.
85 M. R. Das, M. Wang, S. Szunerits, L. Gengembre and R. Boukherroub, *Chem. Commun.*, 2009, 2753.
86 A. W. Taylor and P. Licence, *ChemPhysChem*, 2012, **13**, 1917–1926.
87 R. A. Vaia, R. K. Teukolsky and E. P. Giannelis, *Chem. Mater.*, 1994, **6**, 1017–1022.
88 W. Wang, L. Li and S. Xi, *J. Colloid Interface Sci.*, 1993, **155**, 369–373.
89 T. Kawai, J. Umemura, T. Takenaka, M. Kodama and S. Seki, *J. Colloid Interface Sci.*, 1985, **103**, 56–61.

90 R. G. Snyder, H. L. Strauss and C. A. Elliger, *J. Phys. Chem.*, 1982, **86**, 5145–5150.
91 S. E. Creager and G. K. Rowe, *J. Electroanal. Chem.*, 1997, **420**, 291–299.
92 J. Song, D. Jańczewski, Y. Ma, M. Hempenius, J. Xu and G. J. Vancso, *J. Mater. Chem. B*, 2013, **1**, 828–834.
93 A. Lee, S. K. Y. Tang, C. R. Mace and G. M. Whitesides, *Langmuir*, 2011, **27**, 11560–11574.
94 J. Bolze, M. Takahasi, J. Mizuki, T. Baumgart and W. Knoll, *J. Am. Chem. Soc.*, 2002, **124**, 9412–9421.
95 M. L. Cortez, M. Ceolín, O. Azzaroni and F. Battaglini, *Anal. Chem.*, 2011, **83**, 8011–8018.

